Surfaces and Interfaces 97 (2026) 110207

Contents lists available at ScienceDirect

Surfaces and Interfaces

journal homepage: www.sciencedirect.com/journal/surfaces-and-interfaces

The role of interfacial oxygen in the nucleation and stability of Ni nanoclusters at MgO ultrathin films: Insights from STM and first-principles DFT calculations

Mirali Jahangirzadeh Varjovi [a,1], Anshika Singh [b,1], Elina Mkrtchian [c,d], Mario Rocca [b,c], Luca Vattuone [b,c], Letizia Savio [c,*], Sergio Tosoni [a,*]

[a] Department of Materials Science, University of Milano-Bicocca, 20125, Milano, Italy
[b] Department of Physics, University of Genova, via Dodecaneso 33, 16146, Genova, Italy
[c] IMEM-CNR, UOS Genova, via Dodecaneso 33, 16146, Genova, Italy
[d] Department of Mathematical, Physical and Computer Sciences, University of Parma, 43124, Parma, Italy

ARTICLE INFO

Keywords:
Ni nanoclusters
STM
DFT
Model heterogeneous catalysts
Surface science
Sintering prevention

ABSTRACT

The interaction between metal nanoclusters and oxide surfaces plays a crucial role in determining the properties of materials for catalytic and electronic applications. Here we present a combined experimental scanning tunnelling microscopy and first-principles calculations study of the nucleation and spatial distribution of Ni nanoclusters grown by deposition of Ni atoms on MgO monolayer films supported on Ag(100) at temperature between 100 K and 300 K. Clusters compatible in size with the magic number 13, 55 and 147 compact icosahedral structures are metallic, but partially oxidized in the contact area with the MgO film. They also show a markedly different spatial distribution with deposition temperature: up to 250 K they sit mainly on flat MgO terraces, while at 300 K they accumulate almost exclusively at the steps. Both effects are caused by the unavoidable presence of oxygen atoms at the MgO/Ag interface, whose concentration decreases dramatically just below room temperature.

1. Introduction

Catalysis plays a fundamental role in the production of goods and energy in contemporary society [1]. Its relevance is steadily increasing as the paradigm shifts toward circular pathways and the exploitation of renewable energy sources [2–4]. In particular, most employed catalytic systems fall under the definition of heterogeneous catalysts, in which the active species is a (more or less) small metal particle anchored on a solid support [5–7]. Reducing the size of a supported metal catalyst to the nanoscale is beneficial for saving precious raw materials, maximizing the mass/activity ratio, and increasing the catalyst activity [8–9]. E.g., a recent Density Functional Theory (DFT) and microkinetic study demonstrated that nickel nanoparticles with 1.7 nm size are expected to have the highest catalytic performance for CO_2 methanation [10].

Catalytic reactions often occur at relatively high temperatures, where sintering may take place. The ability to control the size and the properties of supported nanoparticles is thus essential for further optimization of the heterogeneous catalyst. In this respect, the interaction with the support plays a significant role. On the one hand, it ultimately controls the stability of the active particles and their tendency to undergo sintering and thermal deactivation [11–17]. Indeed, it was shown that Ag clusters stop sintering at a diameter of 6 nm on MgO but only of ~3 nm on Ceria [18]. On the other hand, chemical and structural changes induced by the support on the metal particles can deeply affect their chemical properties and reactivity.

It is thus interesting to complement applied studies in catalysis, where the activity and turnover frequency of a given system are the main figures of merit, with more basic works, aimed at the thorough characterization of the structural properties of supported metal nanoparticles and their interaction with the support. This eventually justifies the effort to grow insulating oxides as ultrathin films on metal surfaces: such systems allow the study of wide-gap oxides (often used as supports in catalytic processes) using electron-based techniques. In particular, high-resolution scanning tunnelling microscopy can be employed,

* Corresponding authors.
E-mail addresses: letizia.savio@cnr.it (L. Savio), sergio.tosoni@unimib.it (S. Tosoni).
[1] These authors contributed equally.

https://doi.org/10.1016/j.surfin.2026.110207
Received 21 May 2026; Received in revised form 15 July 2026; Accepted 23 July 2026
Available online 24 July 2026
2468-0230/© 2026 The Author(s). Published by Elsevier B.V. This is an open access article under the CC BY license (http://creativecommons.org/licenses/by/4.0/).

exploiting the electron tunnelling effect enabled by the extreme thinness of the oxide film [19,20]. However, ultra-thin oxide films exhibit peculiar chemical and physical properties, distinguishing them from their bulk counterparts [20–23]. In particular, magnesium oxide (MgO) has attracted remarkable attention due to its good lattice match with metal supports such as silver (Ag) and molybdenum (Mo), enabling the epitaxial growth of ordered films [24]. Additionally, it was reported that the electron transfer via tunnelling through the MgO film induces the formation of negatively charged, highly reactive sub-nanometric Au particles [25,26].

Despite the relative structural simplicity of the interface between rock salt MgO and the Ag(100) cubic lattice, numerous papers have shown that the preparation conditions remarkably influence the morphology of the films. For instance, several reports describe the formation of MgO bilayers epitaxially grown on Ag(001) [27], while some of us reported and characterized the formation of extended monolayers [28]. Notably, given the non-negligible oxophilicity of silver [29], a certain concentration of oxygen is unavoidably trapped at the MgO/Ag interface during the growth process, with relevant impact on the work function of the system and on interfacial charge transfer phenomena. Its optimal concentration was estimated as 25 % recurring to ab initio thermodynamics, in good agreement with the value of 30 % estimated experimentally at 200 K [30]. However, regions with different loading of interfacial oxygen (O_{int}) can form during the growth process underneath any given MgO island [31]. Such interfacial oxygen can diffuse to the external layer leading to a complete oxidation of the smallest nickel aggregates (in the range of 4–6 atoms) under ultra-high vacuum conditions [32].

Larger Ni aggregates on MgO/Ag(100) are, on the contrary, mainly metallic [33]. DFT calculations recently performed by some of us showed that such clusters are slightly negatively charged in the absence of O_{int} whereas they assume a slightly positive charge in its presence. This positive charge may increase significantly due to a thermodynamically favourable reverse oxygen spillover phenomenon leading O atoms to diffuse from the MgO/Ag interface through the MgO film and bind to the Ni clusters [34]. This is an important observation, since the oxidation state of Ni particles, often observed for real catalytic systems under operando conditions, strongly influences their chemical reactivity [35–43].

In the present paper, we shall demonstrate by comparing experimental data with DFT calculations that these Ni nanoclusters (NCs) indeed have an oxidized root and that the interfacial oxygen concentration determines their spatial distribution at terrace and step sites of the MgO film. These findings are of high importance for the rational design of heterogeneous catalysts, where the strength of the adhesion to the support dictates the activity of the supported particles, and their resistance toward sintering and thermal deactivation [44].

2. Experimental and theoretical section

Experiments were carried out in an ultrahigh vacuum system hosting a LT-STM (Createc) and connected to a preparation chamber equipped with a Knudsen cell and an O_2 doser for reactive Mg evaporation, a quartz microbalance (QMB) for Mg flux measurements, an e-beam evaporator (Focus EFM 3) mounting a high-purity (99.99 %) Ni rod, and with additional facilities for sample cleaning and residual gas analysis.

The Ag(100) substrate is a single crystal cut within 0.1° off the high symmetry plane. Before each experiment, the sample is carefully cleaned by sputtering with Ne^+ ions followed by annealing to a temperature T = 850 K for 5 min. Surface cleanliness and order were checked by STM. Monolayer MgO films were grown by reactive deposition at T = 773 K, followed by post-annealing in O_2 atmosphere and slow cooling to T < 450 K [28]. Mg was evaporated from a crucible at T_{ev}=593 K, providing an Mg flux of ~1 Å/min., in an O_2 pressure P_{O2}= 1 × 10^{-6} mbar; however, since the oxygen was introduced in the preparation chamber through a doser placed at ~2 cm from the Ag(100) surface, an effective pressure at least five times higher is expected [45]. Ni was deposited on the MgO/Ag(100) sample at 100 K≤T ≤ 300 K in a background pressure better than 2 × 10^{-9} mbar. The Ni flux could not be measured during evaporation, so the total Ni coverage is evaluated a posteriori from analysis of STM images, accounting for the different sizes and shapes of the clusters at different deposition temperatures.

Samples are cooled to T < 150 K and inserted into the STM immediately after preparation. STM images were recorded at liquid nitrogen temperature with a Pt/Ir tip cut in air under strain and then reshaped by controlled crashes into the surface, so that tunnelling effectively occurs through an Ag tip. The images were acquired in constant current mode, with typical tunnelling currents of ~ 0.2 nA and bias voltage applied to the sample, −4.0 V ≤ V ≤ +4.0 V. The lateral size of the images and the orientation of the surface are determined from atomically resolved measurements of the clean Ag(100) surface (as the one reported in Fig. 1f); similarly, heights are calibrated against monatomic Ag steps. STM analysis was performed with the help of WSxM software [46].

In this study, all first-principles calculations were performed within the framework of spin-polarized DFT [23,24,47,48] as implemented in the Vienna Ab initio Simulation Package (VASP) [25–27,49–53]. The exchange-correlation potential was parameterized using the Perdew–Burke–Ernzerhof (PBE) [54] functional within the generalized gradient approximation (GGA). The projector-augmented wave (PAW) [55] method was employed to describe the pseudopotentials for O, Mg, Ni, and Ag. A kinetic energy cutoff of $\frac{\hbar^2|K+G|^2}{2m} = 520\ eV$ was employed for the plane-wave basis set, and a vacuum space of ~20 Å was inserted in the non-periodic direction for all calculations involving clusters on different supports to prevent artificial interactions between neighbouring images. Brillouin zone (BZ) sampling for the relaxation of the MgO (100) monolayer and Ag(100) slab was performed using a Γ-centred 8 × 8 × 1 uniform k-point mesh [56]. For the optimization of NCs on various supports, VASP-Γ was employed with a 1 × 1 × 1 k-point grid, suitable for the large supercell sizes. Bader charge analysis was employed to obtain the net charge transfer between the clusters and the supports [57]. During total energy calculations, the electronic relaxation converged to a threshold of 10^{-5} eV between consecutive steps. The optimization of ionic positions and lattice constants was performed until the maximum force on each atom was below 0.01 eV/Å. Furthermore, long-range dispersion effects were considered using the D3 method from Grimme, which includes the Becke-Johnson damping function [58,59]. The magnetic configuration for all calculations was initialized consistently, with a singlet state for Mg, O, and Ag, and a triplet state for Ni, while allowing the configuration to evolve during the self-consistent field iterations. The adsorption energy of the nanoclusters (E_{ads}) can be computed via the following formula

$$E_{ads} = E(Ni_X / Support) - -E(Ni_X) - -E(Support) \quad (1)$$

where E(Ni_X /Support) represents the total energy of the examined systems, E(Ni_X) and E(Support) denote the total energies of the gas-phase NCs and the support, respectively, and x indicates the number of Ni atoms within the cluster (x = 13, 55, 147).

3. Nucleation and migration of Ni nanoclusters

Fig. 1a-d shows STM images of Ni NCs grown on monolayer MgO/Ag (100) at four different temperatures: a) 100 K, b) 200 K, c) 250 K and d) 300 K. The protocol followed for the growth of the MgO monolayer is the one reported in ref [28], leading to extended MgO islands limited only by the size of the Ag terrace underneath. Ni atoms are eventually evaporated by e-beam evaporation. After deposition, they aggregate forming Ni clusters. At 200 K, one-third of the Ni coverage consists of small Ni_xO_y clusters (4≤x ≤ 6) while the rest aggregates into larger, metallic clusters [33]. At 300 K only the larger clusters form. Their apparent average diameter increases thereby from 10–12 Å at 100 K to 17–20 Å at 300 K. A qualitatively similar increase in the Ni/MgO contact

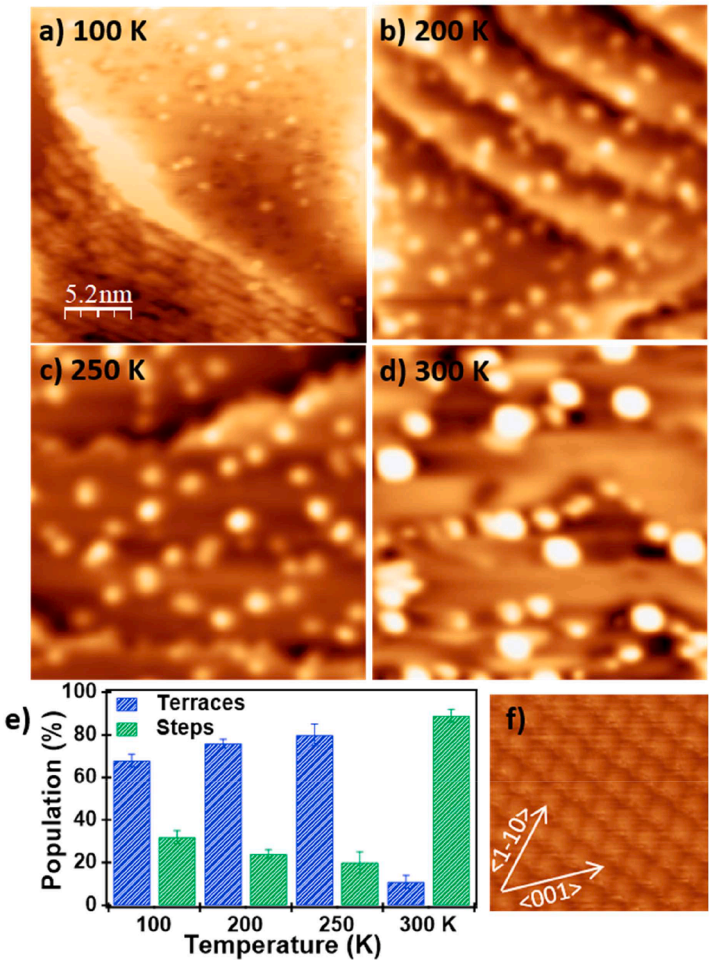


Fig. 1. STM images of Ni NCs deposited at different temperatures on monolayer MgO/Ag(100). a) T = 100 K, b) T = 200 K, c) T = 250 K, and d) T = 300 K. For all images, size: 26 × 26 nm^2; V =+1.0 V. e) Population of clusters at steps and terraces as a function of temperature. The percentages reported in the histogram and in the text are averaged over a minimum of several STM images of size (26 × 26) nm^2 (10 images at 100 K, 13 images at 200 K, 5 images at 250 K and 11 images at 300 K). The standard error is reported. f) Atomically resolved image of the clean Ag(100) substrate, from which the high symmetry directions (marked by arrows) and the calibration parameters are deduced.

area (while the cluster height is conversely reduced) was also noticed by means of Ab-Initio Molecular Dynamics simulations, comparing structures simulated at 0 K and 200 K [34]. Incidentally, dark spots are visible in Fig. 1a. An ultimate assignment on their nature cannot be provided, but we report that changes in contrast within MgO islands were previously attributed to non-uniform distribution of interfacial oxygen, affecting the local density of states of the MgO film [31].

As evident at a first glance from Fig. 1a-d and from the histogram of Fig. 1e), the distribution of Ni nanoclusters at MgO steps or terrace sites strongly depends on the deposition temperature: for T ≤ 250 K, they are found mainly at terraces, while at 300 K, they decorate the steps. Indeed, the relative population of NCs at step sites is between 20 and 30 % for T ≤ 250 K but it jumps to (89 ± 3) % at 300 K (see Table S1 in Supporting Material).

Formation of metal nanoparticles of larger diameter and the preferential population of clusters at steps with increasing temperature have also been reported for other systems, such as Cu atoms deposited on $CeO_{1.95}$(111) and Au clusters on NaCl(001) [60,61]. This behaviour can be rationalized by considering that, at low T, diffusion is slow and the metal atoms have a high probability of meeting another atom/cluster and aggregating before reaching a step. Although diffusion certainly also plays a role in the present case, the trend in relative population does not show any preferential nucleation at steps below 300 K, even though nanometric clusters grow also at lower temperature. The overviews in Fig. 1 a-c may appear different, but this is mainly due to the different step density of the imaged MgO areas since statistical analysis over several images (Fig. 1e) indicates a similar population of Ni NCs at steps for T ≤ 250 K. Vice versa, the outcome at 300 K suggests the activation of a different mechanism. As it will be discussed in the following, our findings envisage that the presence of interfacial oxygen between MgO and Ag could enhance the clusters stability on terraces. The limited thermal stability of O_{int}, though, may explain the preferential growth at steps at 300 K. We also remark that alternative explanations as the presence of F-centres or OH acting as nucleation centres at the terraces at low temperature can be excluded. On the one hand, oxygen vacancies are unlikely in the presence of O_{int}; on the other hand, the presence of OH is ruled out by vibrational spectroscopy analysis performed during CO exposure on Ni NC/MgO/Ag(100) [33].

To gain more insight into this phenomenon, we performed DFT modelling of particles of comparable size to those observed in the STM measurements. First, we note that the measured cluster diameter should be corrected for convolution with the STM tip, so that a size in the range of 5 nm to 15 nm can be inferred. Given the highly complex polymorphism and the actual composition of supported metal clusters within the observed size range, we decided to focus on specific clusters exhibiting high stability in the gas phase. Therefore, we chose the icosahedral Ni_{13}, Ni_{55} and Ni_{147} clusters, corresponding to the "magic numbers" for which the nanoparticles exhibit complete outer atomic

shells and compact structures [62]. It must be stated, however, that other geometries could as well be possible, and an exhaustive study of the polymorphism in supported particles is beyond the scope of the present work.

As shown in Fig. S1 of the Supporting Material, they are all characterized by triangular closed packed nanofacets; in the gas phase their diameter spans from 4.67 Å (Ni_{13}), to 9.24 Å (Ni_{55}), and to 13.93 Å (Ni_{147}) (see Table 1).

The adsorption of these clusters was simulated on the various MgO supports on Ag(100) schematized in Fig. S2: a continuous MgO monolayer (ML_c, panel a), a finite monolayer MgO island (ML_i, panel b), a continuous MgO bilayer (BL_c, panel c), and a stepped MgO BL (BL_s, panel d).

The results of the simulations are reported in Table 1. The side views of the corresponding relaxed structures are shown in Fig. 2. First, one can notice that the icosahedral clusters maintain a quasi-spherical geometrical arrangement on all MgO supports: their height with respect to the surface (measured as the difference in the z coordinate between the apical Ni atom of the cluster and the basal MgO plane) and their diameter display very similar values (Table 1, col. III and IV). On ML_i, the clusters sit at the edge of the MgO island, in contact with the bare Ag. In this case, Ni_{55} and Ni_{147} clusters retain their quasi-spherical shape, while the Ni_{13} ones wet the bare metal. We remark that, in general, the calculated physical heights exceed the values previously reported in ref [33]; however, the latter ones correspond to the apparent height measured by STM, so that a direct comparison is misleading. The clusters' magnetization (Table 1, col. V) does not undergo drastic changes relative to the gas-phase, with a general small increase (Ni_{13}) or small decrease (Ni_{55} and Ni_{147}). Ni_{13} maintains an almost neutral charge state upon adsorption on the various MgO supports featured in Fig. 2. At the same time, Ni_{55} and Ni_{147} acquire a sizable negative charge, with little difference on MLs or BLs (col. VI). Interestingly, the interfacial dipole (col. VII) does not correlate with such a charge transfer: if negative charge is injected into a metal cluster adsorbed on the surface, a positive dipole moment would be expected; however, neither its sign nor its intensity shows a regular trend. This could be explained by an internal compensation effect among the dipole moment generated at the MgO/Ag interface, the contribution of charge transfer to the adsorbed Ni cluster, and charge redistribution phenomena within the metal particle.

Notably, a clear trend in the adsorption energy emerges for clusters of all sizes (Table 1, col. VIII): the strongest adhesion (corresponding to the most negative values of E_{ads}) is observed on the stepped BL, followed by the continuous ML, the continuous BL, and the stepped ML. This clearly shows the remarkable action as trapping sites exerted by the MgO steps. The stronger adhesion on continuous MLs compared to continuous BLs could be ascribed to two factors: i) a stabilizing hybridization of the electron densities of the Ni atoms with the silver atoms, enabled by the extreme thinness of the MgO film, and ii) the larger work function of the continuous MgO ML/Ag compared to MgO BL/Ag, which could affect the charge injection to the Ni particle, strengthening the bond. The stronger binding of metal species on ML compared to BL has been previously observed for single atoms [63]. Finally, it is worth noting that the MgO ML/Ag interface is not an efficient trapping site. Indeed, all the clusters show the lowest E_{ads} on the ML_i substrate. Probably the stronger bonding between the truncated ML borders and the Ag substrate reduces site reactivity with respect to the stepped BL. We remark, however, that the BL_s model best reproduces our experimental conditions at step sites, where a monolayer MgO film covers both the top and the bottom terraces at the steps, with no Ag exposed.

Therefore, our calculations predict that the model of Fig. 2d is the most stable among the investigated ones, and Ni clusters are expected to decorate MgO steps. However, this result contrasts with the experimental data, showing a significant population of terraces at $T \leq 250$ K. The failure of the model in reproducing the experimental results indicates that an important parameter has been overlooked. Considering the role of interfacial oxygen in the growth of ordered MgO monolayers and in the spontaneous oxidation of ultrasmall Ni clusters, we focused our attention on the presence of O_{int}, and we included it in the calculations [28–32].

Table 1
Ni_X (X = 13, 55, 147) adsorbed on a continuous MgO ML/Ag (ML_c), an MgO ML island on Ag (ML_i), a continuous MgO BL/Ag (BL_c), and a stepped MgO BL/Ag (BL_s). Columns III to VIII refer, respectively, to cluster height with respect to the basal plane (h, Å), cluster diameter (d, Å), magnetization (μ, μ_B), Bader charge (Q, |e|), interfacial dipole moment (dip, |e| × Å), and adsorption energy (E_{ads}, eV).

I Support	II Ni_x	III h (Å)	IV d (Å)	V μ (μ_B)	VI Q (|e|)	VII dip (|e| × Å)	VIII E_{ads} (eV)
Gas-phase	13	-	4.67	8.00	-	-	-
	55	-	9.24	39.94	-	-	-
	147	-	13.93	99.19	-	-	-
ML_c	13	5.68	4.80	8.97	−0.11	−3.46	−5.39
	55	9.38	9.23	36.63	−0.89	−1.50	−8.46
	147	13.42	13.95	96.58	−1.47	+0.03	−12.12
ML_i	13	3.62	4.79	8.67	−0.02	−1.32	−5.10
	55	9.39	9.29	37.87	−0.67	+0.03	−7.25
	147	13.66	13.96	96.51	−1.07	+0.87	−9.65
BL_c	13	5.94	4.78	8.35	−0.27	−4.51	−5.14
	55	9.98	9.32	36.78	−1.63	−1.80	−7.78
	147	13.74	13.97	95.32	−2.55	+0.07	−11.37
BL_s	13	5.53	5.65	9.45	+0.10	−3.77	−8.22
	55	10.21	9.62	37.01	−1.30	−1.75	−9.71
	147	13.61	13.96	95.03	−2.22	−0.04	−15.39

4. Effect of the interfacial oxygen and clusters oxidation

The effect of adding oxygen at the interface in the computational models is shown in Fig. 3 and Table 2 for the three most interesting cases previously described: continuous ML (ML_c_O), continuous BL (BL_c_O), and stepped BL (BL_s_O). In the models we assume 25 % coverage of interfacial oxygen, corresponding to the optimal concentration reported in our previous work [30]. Partial oxidation of the Ni atoms in contact with the MgO film occurs, leading to global stabilization of the clusters, an effect that is more pronounced for the smallest nanoparticles. The observed clusters are indeed compatible with the presence of an oxide root as shown in the Supporting Material (Fig. S3).

The data in Table 2 highlight the strong effect of O_{int} on the MgO surface physical and chemical properties and on the MgO interaction with Ni clusters. In particular, the main structural parameters of the adsorbed Ni_X are only marginally affected: comparing Table 1 and Table 2 one can notice only a negligible or small decrease in the physical height of the clusters (col. III). Vice versa, relevant changes are observed in the electronic and magnetic properties, as well as the adhesion strength and relative stability on the various supports. In general, the magnetization of Ni_X (col. V) is significantly larger on supports bearing 25 % O_{int}, in particular on ML_c_O and BL_s_O. For the continuous MgO bilayer (BL_c_O), the effect is less pronounced. The change in the magnetization is related to an inversion of the charge state of the supported clusters that display negative charge on ML_c and BL_s (Table 1, col. VI) and positive (and generally larger) charge on ML_c_O and BL_s_O (Table 2, col. VI), in agreement with previous findings by some of us [34]. Interestingly, the effect is much smaller on BL_c_O, where the charge of the supported Ni clusters is negative (though less negative than in the absence of O_{int}, Table 1) or almost neutral. Steps, thus, represent an intermediate case between ML terraces, where the stabilization exerted by O_{int} on metal clusters is very strong, and BL terraces, where the effect is very weak.

In general, in the presence of interfacial oxygen, the adsorption energy is remarkably larger on all types of MgO supports (Table 2, col. VIII). However, this enhancement in stability is much stronger in ML_c_O

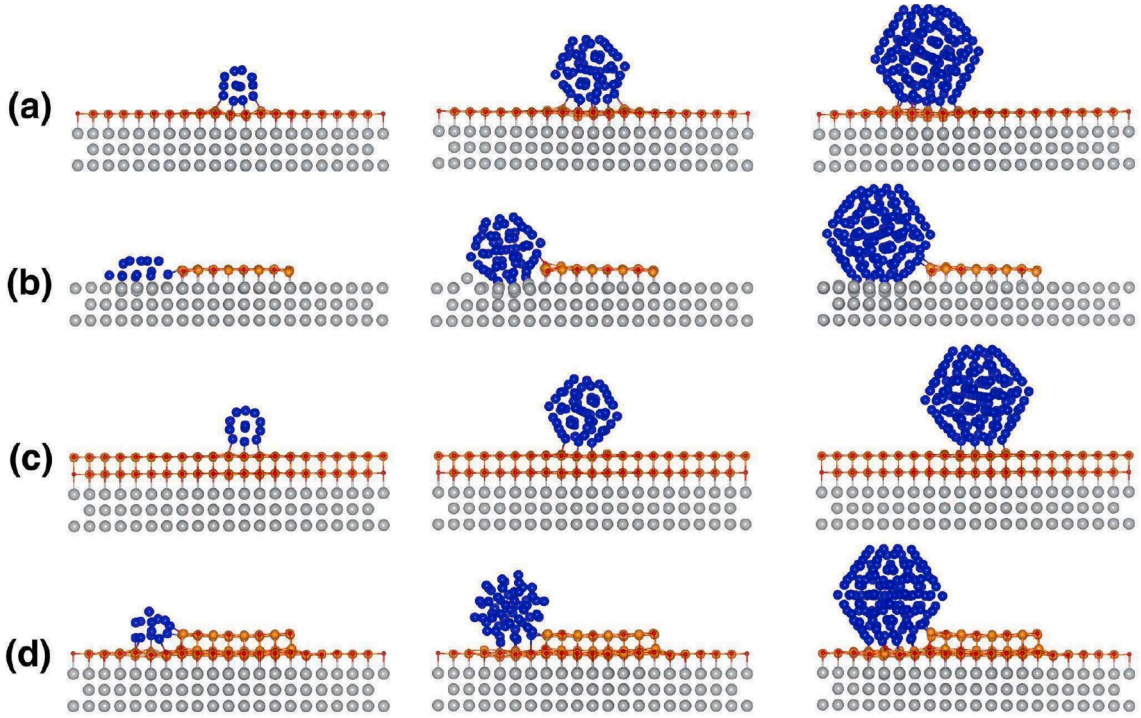


Fig. 2. Side views of the calculated structures of Ni clusters on a) ML_c, b) ML_i, c) BL_c, d) BL_s.

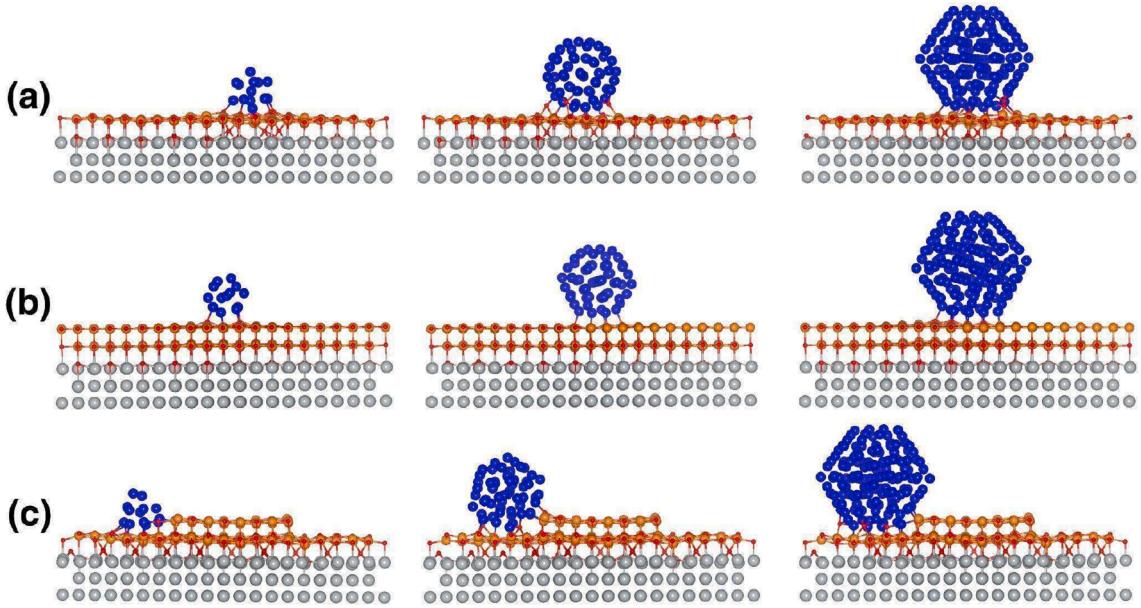


Fig. 3. Side views of the calculated structures of Ni clusters on a) ML_c_O, b) BL_c_O, c) BL_s_O.

than in MgO bilayers and it affects the overall stability trend. Indeed, in the presence of interfacial oxygen, the clusters are bound more strongly on continuous ML terraces (ML_c_O) than at bilayer steps (BL_s_O) and this behaviour is opposite to the one predicted in the absence of O_{int} (compare ML_c and BL_s in Table 1, col. VIII).

The different effect of an analogous concentration of interfacial oxygen on MgO MLs and BLs can be attributed to the different thickness of the insulating MgO layers. As expected, the effect of O_{int} is smaller on thicker BLs compared to MLs.

We can now explain the effect of deposition temperature on the cluster distribution observed in the STM experiments using these DFT results. Firstly, we recall that Ni clusters on monolayer MgO terraces are best modelled by Ni_X adsorption on the ML_c or ML_c_O supports, whereas BL_s or BL_s_O are more suitable for representing cluster adsorption on the MgO steps. DFT clearly indicates the essential role of interface oxygen concentration and of its temperature dependence. Indeed, the presence of aggregations larger than few-atoms at 100 K already, in agreement with previous reports [33], is a key-point in indicating the presence of a mechanism acting beyond bare thermally enhanced diffusion. On the other hand, theory predicts that, in the absence of interfacial oxygen, the Ni clusters are most stably adsorbed at MgO steps of the BL_s supports. In contrast, in the presence of O_{int},

Table 2
Ni_X (X = 13, 55, 147) adsorbed on MgO/O/Ag (bearing 25 % O_{int} at the MgO/Ag interface). Calculated values for the continuous MgO ML/O/Ag (ML_c_O), continuous MgO BL/O/Ag (BL_c_O), and stepped BL/O/Ag (BL_s_O) supports are reported. Columns III to VIII refer, respectively, to cluster height with respect to the basal plane (h, Å), cluster diameter (d, Å), cluster magnetization (μ, μ_B), Bader charge (Q, |e|), interfacial dipole moment (dip, |e| × Å), and adsorption energy (E_{ads}, eV).

I Support	II Ni_x	III h (Å)	IV d (Å)	V μ (μ_B)	VI Q (|e|)	VII dip (|e| × Å)	VIII E_{ads} (eV)
ML_c_O	13	5.47	4.77	10.69	+0.91	−1.42	−23.36
	55	9.12	9.27	40.14	+1.78	−0.57	−28.77
	147	13.20	13.96	100.14	+1.92	+0.55	−32.65
BL_c_O	13	6.02	4.86	9.58	+0.48	−2.08	−8.22
	55	9.79	9.31	37.96	−0.08	−0.62	−7.95
	147	13.66	14.02	97.86	−0.02	+0.32	−11.91
BL_s_O	13	5.63	6.15	11.79	+1.41	−0.52	−15.53
	55	10.17	9.67	38.93	+1.33	+0.19	−17.28
	147	11.52	14.42	97.29	+1.91	+0.87	−23.12

partial oxidation and adsorption on ML terraces (ML_c_O) is favoured.

Therefore, we can rationalize the different spatial distribution of Ni clusters vs growth temperature considering that for T ≤ 250 K there is enough interfacial oxygen for the clusters to get partially oxidized and anchor at terraces; vice versa, at T = 300 K the O_{int} concentration is depleted and MgO steps become the most favourable adsorption site.

This picture is supported by the calculation of the O_{int} free energy at P = 1 × 10^{-9} mbar and T = 100–400 K (see Table S2 in the Supporting Material), i.e. in conditions close to the experimental ones for Ni clusters growth. At 25 % O_{int} coverage, Ni NCs are stable on all supports, with a trend in binding energy that is ML_c ≈ BL_c > BL_s. However, the adsorption energy values decrease with increasing temperature, becoming almost negligible at 400 K. Experimentally, an estimate of O_{int} is available only at 200 K but, considering that comparison with DFT calculations are only qualitative, it is reasonable to suppose that the stability of O_{int} is negligible already at RT [28]. It is also interesting, in this respect, to mention that the different O_{int} stability in ML_c and BL_c (i.e. in the central region of MgO islands) compared to steps could induce oxygen diffusion within the MgO/Ag interface. Overall, the O_{int} concentration can vary due to various factors; direct evaporation of oxygen is unlikely under the observed experimental conditions but reverse oxygen spillover or diffusion into the subsurface Ag(100) region must be considered. Reverse oxygen spillover from the MgO/Ag interface to the external surfaces of the adsorbed Ni clusters was recently proved to be strongly thermodynamically favoured for Ni_{55} clusters by DFT calculations. It implies a concerted mechanism in which O atoms from the MgO lattice move to the Ni cluster borders and the oxygen vacancies are refilled by interfacial oxygen species [34]. It was not possible, though, to evaluate the actual diffusion barrier for this process. From the experimental point of view, the deposition of Ni adatoms takes place in ultrahigh vacuum so that O_{int} is the only oxygen reservoir available for the observed formation of NiO_x clusters [32]. It is thus possible that, in the initial stage of nucleation and growth of the clusters, concomitant partial oxidation takes place, as also supported by the analysis of the shapes and height profiles in the STM images reported in the Supporting Material, and the occasional identification of the previously described Ni_xO_y oligomers [32]. At higher temperatures, the kinetic barriers hindering this mechanism will be more easily overcome. This effect, combined with the higher mobility of deposited Ni atoms, contributes to explaining the change in the clusters' size and spatial distribution observed at room temperature. The diffusion of partially oxidized Ni_xO_y entities could, in principle, also contribute to further non-trivial growth mechanisms.

The diffusion of the interfacial oxygen back into the Ag subsurface is difficult to monitor experimentally. Some of us demonstrated, using photoelectron spectroscopy, that a subsurface oxygen species migrates into the bulk at T > 280 K on O/Ag(210) [64]. However, the situation is different if oxygen is trapped at the MgO/Ag interface, so that we must rely on DFT calculations showing that diffusion into the Ag bulk is thermodynamically unfavourable (see Supporting Material, Fig. S4). The most probable fate of the subsurface oxygen is therefore its migration into the larger Ni clusters forming at RT.

Finally, we remark that the diffusion barrier for such clusters is expected to be around 1/3 of their adsorption energy, which implies that they should not sinter at temperatures lower than 600 K. This agrees well with the size distribution of the grown nanoparticles, having a diameter between 1.0 and 1.5 nm, i.e. compatible with the size of Ni_{55} and Ni_{147}, and demonstrates the active role of a suitable substrate in the optimization of catalytic materials [33]. This result is potentially quite appealing to obtain nanoparticles of kinetically limited shape under temperature conditions which are considered the optimal ones for CO_2 methanation on non-reducible oxide supports (640 K according to ref [10]). It must be stated, though, that the catalytic operating conditions do not envisage only high temperature, but also exposure to high pressure of reactive gases such as oxygen, hydrogen, CO_2 and others. Our previous computational work [34] assesses the stability of supported Ni clusters in an oxidizing environment, but their behaviour under reducing conditions and exposure to reactive gases remains to be investigated.

5. Conclusions

In this study we show that the nucleation, spatial distribution and thermal stability of Ni nanoclusters on MgO/Ag(100) surfaces are strongly influenced by the morphology of the substrate by using STM analysis and DFT calculations.

The MgO/Ag interface acts as a reservoir releasing O in oxygen poor conditions or segregating it under oxygen rich conditions. The observed nucleation pattern highlights the combined role of interfacial oxygen and diffusion kinetics in directing cluster growth. Furthermore, stability analysis reveals that Ni clusters retain their structural integrity within a definite size regime, while the migration to steps observed at 300 K could further lead to agglomeration. These results provide fundamental insights into metal oxide/interface behaviour and open pathways for tailoring Ni NCs for catalysis and nanoscale devices.

CRediT authorship contribution statement

Mirali Jahangirzadeh Varjovi: Writing – review & editing, Writing – original draft, Methodology, Investigation, Formal analysis, Data curation. **Anshika Singh:** Writing – review & editing, Writing – original draft, Methodology, Investigation, Formal analysis, Data curation. **Elina Mkrtchian:** Writing – review & editing, Investigation. **Mario Rocca:** Writing – review & editing, Writing – original draft, Investigation, Funding acquisition, Conceptualization. **Luca Vattuone:** Writing – review & editing, Investigation. **Letizia Savio:** Writing – review & editing, Writing – original draft, Methodology, Investigation, Funding acquisition, Formal analysis, Data curation, Conceptualization. **Sergio Tosoni:** Writing – review & editing, Writing – original draft, Methodology, Investigation, Funding acquisition, Formal analysis, Data curation, Conceptualization.

Declaration of competing interest

The authors declare that they have no known competing financial interests or personal relationships that could have appeared to influence the work reported in this paper. The authors declare no conflicts of interest.

Acknowledgements

We thank Jagriti Pal for participating in the initial stages of STM

experiments.

We acknowledge funding from the European Union – NextGenerationEU, Mission 4, Component 1, through the Italian Ministry of University and Research under projects PRIN-PNRR P20227XSAH, CUP B53D23028390001 and project PRIN 2022 2022LS74H2, CUP B53D23013810006.

Computational support from CINECA supercomputing centre is kindly acknowledged.

Supplementary materials

Supplementary material associated with this article can be found, in the online version, at doi:10.1016/j.surfin.2026.110207.

Data availability

Data will be made available on request.

References

[1] M. Monai, M. Gambino, S. Wannakao, B.M. Weckhuysen, Propane to olefins tandem catalysis: a selective route towards light olefins production, Chem. Soc. Rev. 50 (20) (2021) 11503–11529.
[2] J. Gong, R. Luque, Catalysis for production of renewable energy, Chem. Soc. Rev. 43 (22) (2014) 7466–7468.
[3] J.R. Lockemeyer, T.L. Lohr, M.A. Reynolds, A. van der Made, Catalysis for the energy transition, ChemCatChem 17 (2025) e00588.
[4] G. Centi, J. Čejka, Needs and gaps for catalysis in addressing transitions in chemistry and energy from a sustainability perspective, ChemSusChem 12 (3) (2019) 621–632.
[5] I. Chorkendorff, J.W. Niemantsverdriet, Concepts of Modern Catalysis and Kinetics, John Wiley & Sons, 2017.
[6] Y. Xia, H. Yang, C.T. Campbell, Nanoparticles For Catalysis, ACS Publications, 2013, pp. 1671–1672.
[7] D. Astruc, Introduction: Nanoparticles in Catalysis, ACS Publications, 2020, pp. 461–463.
[8] U. Heiz, E.L. Bullock, Fundamental aspects of catalysis on supported metal clusters, J. Mater. Chem. 14 (4) (2004) 564.
[9] E. Bus, R. Prins, J.A. van Bokhoven, Origin of the cluster-size effect in the hydrogenation of cinnamaldehyde over supported Au catalysts, Catal. Commun. 8 (9) (2007) 1397–1402.
[10] E.B. Sterk, A.-E. Nieuwelink, M. Monai, J.N. Louwen, E.T. Vogt, I.A. Filot, B. M. Weckhuysen, Structure sensitivity of CO_2 conversion over nickel metal nanoparticles explained by micro-kinetics simulations, JACS Au. 2 (12) (2022) 2714–2730.
[11] O. Dulub, W. Hebenstreit, U. Diebold, Imaging cluster surfaces with atomic resolution: the strong metal-support interaction state of Pt supported on TiO_2(110), Phys. Rev. Lett. 84 (16) (2000) 3646–3649.
[12] S. Tauster, Strong metal-support interactions, Acc. Chem. Res. 20 (11) (1987) 389–394.
[13] Z.-H. Qin, M. Lewandowski, Y.-N. Sun, S. Shaikhutdinov, H.-J. Freund, Morphology and CO adsorption on platinum supported on thin Fe3O4(111) films, J. Phys.: Condens. Matter. 21 (13) (2009) 134019.
[14] M. Lewandowski, Y.-N. Sun, Z.-H. Qin, S. Shaikhutdinov, H.-J. Freund, Promotional effect of metal encapsulation on reactivity of iron oxide supported Pt catalysts, Appl. Catal. A: Gen. 391 (1–2) (2011) 407–410.
[15] J.Y. Park, L.R. Baker, G.A. Somorjai, Role of hot electrons and metal–oxide interfaces in surface chemistry and catalytic reactions, Chem. Rev. 115 (8) (2015) 2781–2817.
[16] T. Lunkenbein, J. Schumann, M. Behrens, R. Schlögl, M.G. Willinger, Formation of a ZnO overlayer in industrial Cu/ZnO/Al_2O_3 catalysts induced by strong metal–support interactions, Angew. Chem. 127 (15) (2015) 4627–4631.
[17] F. Polo-Garzon, T.F. Blum, Z. Bao, K. Wang, V. Fung, Z. Huang, E.E. Bickel, D.-E. Jiang, M. Chi, Z. Wu, In situ strong metal–support interaction (SMSI) affects catalytic alcohol conversion, ACS Catal. 11 (4) (2021) 1938–1945.
[18] J.A. Farmer, C.T. Campbell, Ceria maintains smaller metal catalyst particles by strong metal-support bonding, Science 329 (5994) (2010) 933–936.
[19] T. Zambelli, J. Wintterlin, J. Trost, G. Ertl, Identification of the "active sites" of a surface-catalyzed reaction, Science 273 (5282) (1996) 1688–1690.
[20] N. Nilius, Properties of oxide thin films and their adsorption behavior studied by scanning tunneling microscopy and conductance spectroscopy, Surf. Sci. Rep. 64 (12) (2009) 595–659.
[21] S. Street, C. Xu, D. Goodman, The physical and chemical properties of ultrathin oxide films, Annu. Rev. Phys. Chem. 48 (1) (1997) 43–68.
[22] J.M. Rondinelli, N.A. Spaldin, Structure and properties of functional oxide thin films: insights from electronic-structure calculations, Adv. Mater. 23 (30) (2011) 3363–3381.
[23] L. Giordano, G. Pacchioni, Oxide films at the nanoscale: new structures, new functions, and new materials, Acc. Chem. Res. 44 (11) (2011) 1244–1252.
[24] G. Pacchioni, H. Freund, Electron transfer at oxide surfaces. The MgO paradigm: from defects to ultrathin films, Chem. Rev. 113 (6) (2013) 4035–4072.
[25] D. Ricci, A. Bongiorno, G. Pacchioni, U. Landman, Bonding trends and dimensionality crossover of gold nanoclusters on metal-supported MgO thin films, Phys. Rev. Lett. 97 (3) (2006) 036106.
[26] F. Calaza, C. Stiehler, Y. Fujimori, M. Sterrer, S. Beeg, M. Ruiz-Oses, N. Nilius, M. Heyde, T. Parviainen, K. Honkala, Carbon dioxide activation and reaction induced by electron transfer at an oxide–metal interface, Angew. Chem. Int. Ed. 54 (42) (2015) 12484–12487.
[27] E. Carrasco, M.A. Brown, M. Sterrer, H.-J. Freund, K. Kwapien, M. Sierka, J. Sauer, Thickness-dependent hydroxylation of MgO(001) thin films, J. Phys. Chem. C 114 (42) (2010) 18207–18214.
[28] J. Pal, M. Smerieri, E. Celasco, L. Savio, L. Vattuone, M. Rocca, Morphology of monolayer MgO films on Ag (100): switching from corrugated islands to extended flat terraces, Phys. Rev. Lett. 112 (12) (2014) 126102.
[29] N. Janulaitis, C.T. Campbell, Predicting adhesion energies of late transition metal nanoparticles to oxide support surfaces using oxide reducibility and metal oxophilicity: toward Predicting catalyst performance, ACS Catal. 15 (9) (2025) 6874–6880.
[30] J. Pal, M. Smerieri, E. Celasco, L. Savio, L. Vattuone, R. Ferrando, S. Tosoni, L. Giordano, G. Pacchioni, M. Rocca, How growing conditions and interfacial oxygen affect the final morphology of MgO/Ag(100) films, J. Phys. Chem. C 118 (45) (2014) 26091–26102.
[31] L. Savio, M. Smerieri, L. Vattuone, S. Tosoni, G. Pacchioni, M. Rocca, Interface oxygen induced internal structures of ultrathin MgO islands grown on Ag(100), J. Phys. Chem. C 124 (16) (2020) 8834–8842.
[32] M. Smerieri, J. Pal, L. Savio, L. Vattuone, R. Ferrando, S. Tosoni, L. Giordano, G. Pacchioni, M. Rocca, Spontaneous oxidation of Ni nanoclusters on MgO monolayers induced by segregation of interfacial oxygen, J. Phys. Chem. Lett. 6 (15) (2015) 3104–3109.
[33] L. Savio, M. Smerieri, J. Pal, E. Celasco, M. Rocca, L. Vattuone, 2D Ni nanoclusters on ultrathin MgO/Ag(100), J. Phys. Chem. C 124 (1) (2020) 482–488.
[34] M. Jahangirzadeh Varjovi, S. Tosoni, DFT investigation of X55 (X= Ni, Pd, and Pt) clusters on ultrathin supported MgO films: evidence of oxygen spillover and relevance for catalytic model studies, J. Phys. Chem. C 128 (50) (2024) 21331–21342.
[35] W. Gac, T. Borowiecki, P. Kowalik, Nickel nanocatalysts for methane steam reforming, Nanotechnol. Catal.: Appl. Chem. Ind. Energy Dev. Environ. Prot. (2017) 401–420.
[36] A. Parmaliana, F. Arena, F. Frusteri, S. Coluccia, L. Marchese, G. Martra, A. Chuvilin, Magnesia-supported nickel catalysts: II. Surface properties and reactivity in methane steam reforming, J. Catal. 141 (1) (1993) 34–47.
[37] S. Schauermann, N. Nilius, S. Shaikhutdinov, H.-J. Freund, Nanoparticles for heterogeneous catalysis: new mechanistic insights, Acc. Chem. Res. 46 (8) (2013) 1673–1681.
[38] A. Cadi-Essadek, A. Roldan, X. Aparicio-Anglès, N.H. De Leeuw, CO_2 and H_2 adsorption and reaction at Nin/YSZ(111) interfaces: a density functional theory study, J. Phys. Chem. C 122 (34) (2018) 19463–19472.
[39] G.I. Siakavelas, N.D. Charisiou, S. AlKhoori, A.A. AlKhoori, V. Sebastian, S. J. Hinder, M.A. Baker, I. Yentekakis, K. Polychronopoulou, M.A. Goula, Highly selective and stable nickel catalysts supported on ceria promoted with Sm_2O_3, Pr_2O_3 and MgO for the CO_2 methanation reaction, Appl. Catal. B: Environ. 282 (2021) 119562.
[40] C.R. Rêgo, P. Tereshchuk, L.N. Oliveira, J.L. Da Silva, Graphene-supported small transition-metal clusters: a density functional theory investigation within van der Waals corrections, Phys. Rev. B 95 (23) (2017) 235422.
[41] W.-S. Dong, K.-W. Jun, H.-S. Roh, Z.-W. Liu, S.-E. Park, Comparative study on partial oxidation of methane over Ni/ZrO_2, Ni/CeO_2 and Ni/Ce–ZrO_2 catalysts, Catal. Lett. 78 (1) (2002) 215–222.
[42] A. Caballero, J.P. Holgado, V.M. Gonzalez-delaCruz, S.E. Habas, T. Herranz, M. Salmeron, In situ spectroscopic detection of SMSI effect in a Ni/CeO_2 system: hydrogen-induced burial and dig out of metallic nickel, Chem. Commun. 46 (7) (2010) 1097–1099.
[43] G.G. Asara, L.O. Paz-Borbón, F. Baletto, Get in touch and keep in contact": interface effect on the oxygen reduction reaction (ORR) activity for supported PtNi nanoparticles, ACS Catal. 6 (7) (2016) 4388–4393.
[44] C.T. Campbell, The energetics of supported metal nanoparticles: relationships to sintering rates and catalytic activity, Acc. Chem. Res. 46 (8) (2013) 1712–1719.
[45] F.C. Henn, M.E. Bussell, C.T. Campbell, A simple means for reproducibly dosing low vapor pressure and/or reactive gases to surfaces in ultrahigh vacuum, J. Vac. Sci. Technol. A: Vac. Surf. Films 9 (1) (1991) 10–13.
[46] I. Horcas, R. Fernández, J. Gomez-Rodriguez, J. Colchero, J. Gómez-Herrero, A. M. Baro, WSXM: a software for scanning probe microscopy and a tool for nanotechnology, Rev. Sci. Instrum. 78 (1) (2007).
[47] W. Kohn, L.J. Sham, Self-consistent equations including exchange and correlation effects, Phys. Rev. 140 (4A) (1965) A1133–A1138.
[48] P. Hohenberg, W. Kohn, Density functional theory (DFT), Phys. Rev. 136 (1964) (1964) B864–B871.
[49] S. Schintke, S. Messerli, M. Pivetta, F. Patthey, L. Libioulle, M. Stengel, A. De Vita, W.-D. Schneider, Insulator at the ultrathin limit: MgO on Ag (001), Phys. Rev. Lett. 87 (27) (2001) 276801.
[50] G. Kresse, J. Hafner, Ab initio molecular dynamics for liquid metals, Phys. Rev. B 47 (1) (1993) 558–561.
[51] G. Kresse, J. Hafner, Ab initio molecular-dynamics simulation of the liquid-metal–amorphous-semiconductor transition in germanium, Phys. Rev. B 49 (20) (1994) 14251–14269.

[52] G. Kresse, J. Furthmüller, Efficiency of ab-initio total energy calculations for metals and semiconductors using a plane-wave basis set, Comput. Mater. Sci. 6 (1) (1996) 15–50.
[53] G. Kresse, J. Furthmüller, Efficient iterative schemes for ab initio total-energy calculations using a plane-wave basis set, Phys. Rev. B 54 (16) (1996) 11169–11186.
[54] J.P. Perdew, K. Burke, M. Ernzerhof, Generalized gradient approximation made simple, Phys. Rev. Lett. 77 (18) (1996) 3865–3868.
[55] P.E. Blöchl, Projector augmented-wave method, Phys. Rev. B 50 (24) (1994) 17953.
[56] H.J. Monkhorst, J.D. Pack, Special points for Brillouin-zone integrations, Phys. Rev. B 13 (12) (1976) 5188–5192.
[57] G. Henkelman, A. Arnaldsson, H. Jónsson, A fast and robust algorithm for Bader decomposition of charge density, Comput. Mater. Sci. 36 (3) (2006) 354–360.
[58] S. Grimme, S. Ehrlich, L. Goerigk, Effect of the damping function in dispersion corrected density functional theory, J. Comput. Chem. 32 (7) (2011) 1456–1465.
[59] S. Grimme, J. Antony, S. Ehrlich, H. Krieg, A consistent and accurate ab initio parametrization of density functional dispersion correction (DFT-D) for the 94 elements H-Pu, J. Chem. Phys. 132 (15) (2010).
[60] T.E. James, S.L. Hemmingson, C.T. Campbell, Energy of supported metal catalysts: from single atoms to large metal nanoparticles, ACS Catal. 5 (10) (2015) 5673–5678.
[61] T. Hynninen, G. Cabailh, A.S. Foster, C. Barth, Defect mediated manipulation of nanoclusters on an insulator, Sci. Rep. 3 (1) (2013) 1270.
[62] T. Rapps, R. Ahlrichs, E. Waldt, M.M. Kappes, D. Schooss, On the structures of 55-atom transition-metal clusters and their relationship to the crystalline bulk, Angew. Chem. Int. Ed. 52 (23) (2013).
[63] S. Tosoni, G. Pacchioni, Bonding properties of isolated metal atoms on two-dimensional oxides, J. Phys. Chem. C 124 (38) (2020) 20960–20973.
[64] L. Savio, A. Gerbi, L. Vattuone, A. Baraldi, G. Comelli, M. Rocca, Monitoring super- and subsurface oxygen on Ag (210) by high energy resolution X-ray photoelectron spectroscopy: subsurface diffusion and segregation, J. Phys. Chem. B 110 (2) (2006) 942–947.